Prolonged Hot Electron Dynamics in Plasmonic-Metal/Semiconductor Heterostructures with Implications for Solar Photocatalysis**

*Joseph S. DuChene, Brendan C. Sweeny, Aaron C. Johnston-Peck, Dong Su, Eric A. Stach, and Wei David Wei**

Abstract: Ideal solar-to-fuel photocatalysts must effectively harvest sunlight to generate significant quantities of long-lived charge carriers necessary for chemical reactions. Here we demonstrate the merits of augmenting traditional photoelectrochemical cells with plasmonic nanoparticles to satisfy these daunting photocatalytic requirements. Electrochemical techniques were employed to elucidate the mechanics of plasmon-mediated electron transfer within Au/TiO_2 heterostructures under visible-light ($\lambda > 515$ nm) irradiation in solution. Significantly, we discovered that these transferred electrons displayed excited-state lifetimes two orders of magnitude longer than those of electrons photogenerated directly within TiO_2 via UV excitation. These long-lived electrons further enable visible-light-driven H_2 evolution from water, heralding a new photocatalytic paradigm for solar energy conversion.

Solar photocatalysis for chemical fuel production represents a promising approach to sustainably satisfy escalating global energy demands.[1] Unfortunately, current photocatalysts exhibit limited solar-to-fuel efficiencies because the lifetimes of photogenerated electron-hole pairs (ps–µs) are often incommensurate with the prolonged timescales required to facilitate photocatalytic reactions (ms–s) at the semiconductor surface.[1,2a] This kinetic discrepancy hinders the realization of efficient photosynthetic devices for solar energy conversion.[1] Recently, the integration of Au or Ag nanoparticles (NPs) into traditional photoelectrochemical (PEC) cells has been shown to endow the plasmonic composite with enhanced photocatalytic performance by utilizing the surface plasmon resonance (SPR) of plasmonic-metal NPs.[2–4] These

SPs predominantly relax non-radiatively via Landau damping, yielding highly energetic "hot" electrons that transiently populate electronic states above the metal Fermi level.[5] When plasmonic-metal NPs are proximal to a semiconductor with a dense manifold of conduction band (CB) states, the hot electrons can be directly injected into the energetically accessible CB levels of the semiconductor.[2,3,5,6] This plasmon-mediated electron transfer (PMET) process constitutes a unique photosensitization strategy enabling these plasmonic NPs to serve as light-harvesting assemblies when anchored to a semiconductor scaffold.[2,3,5]

Although PMET occurs on an ultrafast timescale ($t < 240$ fs),[6a] the temporal evolution of these transferred electrons within the semiconductor CB after PMET deserves further study. The average lifetime of hot electrons within the semiconductor CB represents an important catalytic parameter, as these photoexcited electrons must persist long enough to facilitate surface reactions.[7] Previous dynamics studies were conducted in air using femtosecond pulsed-laser excitation,[6a,b] and thus did not adequately capture the excited-state dynamics relevant to PEC systems operating in solution.[8] Knowledge of these hot electron dynamics within a plasmonic device under simulated solar conditions is therefore crucial to the further optimization and eventual exploitation of the PMET process in artificial photosynthetic constructs.

To that end, we used a plasmonic PEC cell to elucidate the PMET mechanism in plasmonic-metal/semiconductor (Au/TiO_2) heterostructures during in situ (i.e. aqueous solution) operation. This device architecture renders the plasmonic composite electronically addressable, providing an ideal platform to probe the PMET process. These PEC studies unambiguously confirm that visible-light excitation of the plasmonic Au/TiO_2 photoanode induces PMET from the Au NPs to the CB of the TiO_2 nanowires (NWs). Significantly, we monitored the excited-state lifetimes (τ_n) of these hot electrons within the semiconductor CB in situ and found that the PMET process yields excited-state electrons with prolonged lifetimes compared to those of electrons excited directly within TiO_2. These long-lived electrons were subsequently harnessed for visible-light-driven hydrogen (H_2) evolution from water, demonstrating the utility of PMET for solar photocatalysis.

A TiO_2 NW array was chosen as the Au NP support to unambiguously assign the visible-light response to the plasmonic NPs, while the semiconductor NW served solely as a conduit for hot electron transport. Moreover, relative to planar semiconductor configurations, this nanowire topology has been shown to improve PEC performance by decoupling the directions for light absorption and charge transport within

[*] J. S. DuChene, B. C. Sweeny, Prof. Dr. W. D. Wei
Department of Chemistry and
Center for Nanostructured Electronic Materials
University of Florida, Gainesville, FL 32611 (USA)
E-mail: wei@chem.ufl.edu

Dr. A. C. Johnston-Peck, Dr. D. Su, Dr. E. A. Stach
Center for Functional Nanomaterials
Brookhaven National Laboratory, Upton, NY 11973 (USA)

the device, while providing an uninterrupted conductive corridor for charge carriers to reach the back contact.[9] Scanning electron microscopy (SEM) showed that the TiO_2 NWs were perpendicularly oriented on the substrate with average lengths (l) of 2.2 ± 0.2 μm and diameters (d) of 200 ± 50 nm (Figure S1a–c). X-ray diffraction (XRD) confirmed that these NWs were monocrystalline and composed of rutile TiO_2 (Figure S1d), as initially reported.[9b] Plasmonic Au NPs ($d = 20 \pm 5$ nm) were then photochemically grafted[10] directly onto the TiO_2 NWs to construct Au/TiO_2 heterojunctions free of surfactants and chemical linkers (see the Supporting Information). A dramatic color change occurred after photodeposition, indicating the presence of plasmonic Au NPs (Figures S2 and S3). SEM analysis revealed that the Au NPs were distributed along the TiO_2 support but were predominantly located at the NW terminus (Figure 1a). Given the
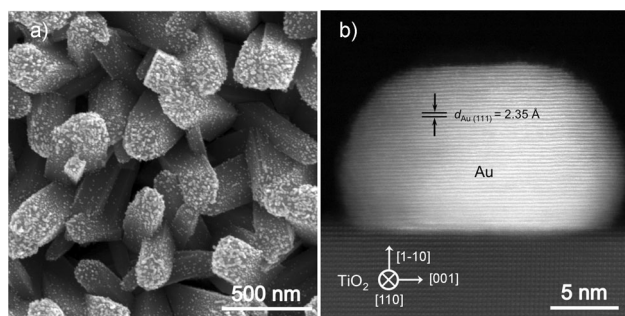
Figure 1. Structural analysis of a typical plasmonic photoanode. a) SEM image of a plasmonic Au/TiO_2 photoanode on the FTO glass substrate. b) HAADF-STEM image demonstrating direct physical contact at the Au/TiO_2 interface ($d_{Au(111)} = 2.35$ Å).

importance of the Au/TiO_2 interface to the PMET mechanism,[2] the heterojunction was further inspected by high-angle annular dark-field scanning transmission electron microscopy (HAADF-STEM). As shown in Figure 1b, a coherent interface was established at the Au/TiO_2 heterojunction, confirming that photodeposition yields the intimate physical contact requisite for PMET.

A suite of PEC experiments were then performed using a three-electrode electrochemical cell consisting of a plasmonic Au/TiO_2 photoanode (working), Pt wire (auxiliary), and Ag/AgCl (reference) electrode all immersed in a supporting electrolyte of 1M NaOH (see the Supporting Information). All electrode potentials (E) are reported relative to the reversible hydrogen electrode (RHE). Chronoamperometry was used to evaluate the PMET process with the plasmonic photoanode potentiostatically poised at $E_{appl} = 1.20\,V_{RHE}$ while being illuminated with periodic (3 s on/off) visible light ($\lambda > 515$ nm). This approach permits the selective excitation of the Au NPs while excluding any contribution from direct interband transitions within the TiO_2 support (Figure S4). As shown in Figure 2a, the plasmonic device exhibits a prompt and reproducible anodic photocurrent (J_{ph}) when exposed to periodic visible-light irradiation. In contrast, the TiO_2-only device produced no J_{ph} under identical conditions (Figure 2a). We therefore attribute the J_{ph} of
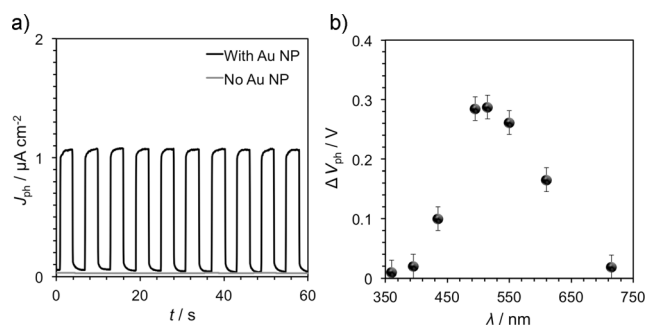
Figure 2. Photoelectrochemical data from TiO_2-only (gray) and Au/TiO_2 (black) photoanodes. a) Chronoamperometry ($J_{ph}(t)$) during periodic visible-light excitation. b) Photovoltage action spectrum difference ($\Delta V_{ph}(\lambda)$) between photoanodes.

1 μA cm^{-2} from the plasmonic device to hot electron injection via optical excitation of the Au NPs.

To further correlate the visible-light activity of the plasmonic photoanode to the optical properties of the Au NPs, the open-circuit voltage (V_{oc}) was monitored as a function of incident photon energy. The occupancy of CB states within a semiconductor during optical excitation is given by the quasi-Fermi level (E_F^*) of the device, which can be monitored externally via the V_{oc} of the PEC cell.[11a] Under open-circuit conditions, the photovoltage (V_{ph}) corresponds to the increase in E_F^* with respect to the equilibrium value obtained in the dark ($E_{F,Redox}$), as given by Equation (1):

$$V_{ph} = \frac{\left(E_{F,n}^* - E_{F,Redox}\right)}{q} = \frac{k_B T}{q} ln\left(\frac{n}{n_0}\right) \tag{1}$$

where $E_{F,Redox}$ corresponds to the Fermi level of the electrolyte, k_B is the Boltzmann constant, T is the temperature (in Kelvin), q is the unsigned charge of an electron, while n and n_0 represent the free electron concentration under illumination and in the dark, respectively.[11] We emphasize that no increase in E_F^* was observed for the TiO_2-only device when it was illuminated with visible light, permitting utilization of the V_{ph} as a PEC probe to monitor the generation of hot electrons in the plasmonic photoanode, as shown in Figure 2b. The V_{ph} difference spectrum ($\Delta V_{ph}(\lambda) = (Au/TiO_2)V_{ph}(\lambda) - (TiO_2)V_{ph}(\lambda)$) reveals a clear distinction between these devices in the visible region assignable to the Au NPs, with the maximum ΔV_{ph} qualitatively corresponding to λ_{max} of the plasmonic device (Figure S2). Taken together, these PEC characteristics conclusively demonstrate that visible-light excitation induces PMET from the Au NPs to the TiO_2 NWs, enabling these plasmonic photoanodes to harvest visible light.

The dynamics of these hot electrons within the TiO_2 CB were then examined in situ by monitoring the temporal profile of the V_{oc} from the plasmonic photoanode while selectively exciting the Au NPs. An extended V_{oc} transient lasting ca. 50 s was observed under $\lambda > 515$ nm irradiation as hot electrons accumulated within the TiO_2 CB, which slowly shifted the V_{oc} of the plasmonic photoanode to more negative potentials (Figure 3a). The extended V_{oc} transient reveals
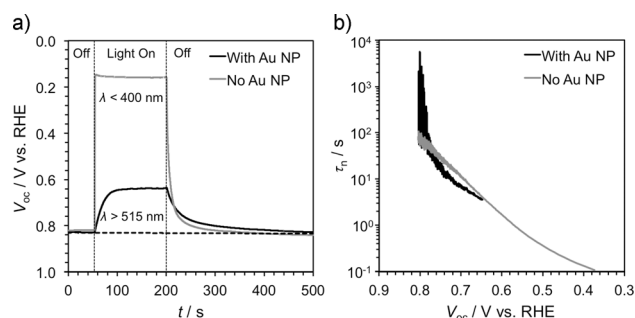
Figure 3. Transient open-circuit voltage decay (OCVD) from the TiO₂-only (gray) and the Au/TiO₂ (black) photoanodes following exposure to UV or visible-light excitation, respectively. a) V_{oc} transient rise/decay obtained during excitation/termination of irradiation. Horizontal dashed black line represents the V_{oc} baseline in the dark. b) Average electron lifetimes (τ_n) within the device.

a limited transmission probability for hot electrons into the TiO₂ CB, strongly suggesting the presence of a Schottky barrier ($\phi \approx 1.0$ eV)[5b–f] at the Au/TiO₂ interface. The relaxation dynamics of these transferred electrons were then monitored immediately after irradiation, and a prolonged V_{oc} decay was observed over several minutes as the CB electrons recombined with any holes trapped on the Au NPs.

The PMET dynamics in the Au/TiO₂ device were distinguished from the intrinsic optical transitions within the TiO₂ support by monitoring the V_{oc} of the TiO₂-only photoanode under UV ($\lambda < 400$ nm) light. As shown in Figure 3a, a substantial distribution of electron-hole pairs was generated via UV excitation of the TiO₂ NWs, and a significant V_{ph} of 0.7 V was promptly established. Upon termination of the UV irradiation, the V_{oc} rapidly decreased back to the equilibrium value obtained in the dark as the CB electrons were scavenged by adsorbed surface species (e.g. dissolved O₂) or relaxed via recombination with holes trapped in the valence band (VB).

Subsequent analysis of these V_{oc} transients via the open-circuit voltage decay (OCVD) method[11] yields the average lifetime of the photogenerated carriers (τ_n) within the device, according to Equation (2):

$$\tau_n = -\frac{k_B T}{q}\left(\frac{dV_{oc}}{dt}\right)^{-1} \tag{2}$$

where τ_n represents the average electron lifetime and all other variables are as previously defined.[11] This measurement preferentially probes the slow recombination kinetics (milliseconds–seconds) of interfacial charge transfer processes occurring at the semiconductor-liquid junction.[11a,b] Consequently, this approach lends unique insight into the extended dynamics of long-lived electrons capable of facilitating reduction reactions, since these processes transpire on similar timescales.[1]

As shown in Figure 3b, the hot electrons transferred to the TiO₂ CB via PMET exhibited lifetimes that were 1–2 orders of magnitude longer ($\tau_n \approx 10^3$ s) than those of CB electrons excited within the TiO₂ NWs themselves ($\tau_n \approx 10^1$ s). Moreover, the relatively short-lived distribution ($\tau_n \approx 0.1$ s)

indicative of rapid recombination was not observed for the hot electrons generated through the PMET mechanism. The absence of these short-lived carriers strongly suggests a reduced recombination rate following the PMET process. It must be recognized that τ_n corresponds to the characteristic lifetimes for both free and trapped electrons within the TiO₂ CB.[11] Although trap states often mediate electron transport within NP-based TiO₂ films,[12] our device is composed of a highly-oriented rutile TiO₂ NW array known to possess a low density of defects.[12b] The photodeposition of Au NPs is further expected to preferentially passivate defects on the TiO₂ surface,[3e, 10] suggesting a diminished contribution from trap states to the lifetimes observed in the Au/TiO₂ device. We emphasize that the lifetimes of CB electrons within the TiO₂-only device are consistent with prior reports;[3e,11c] however, the singular nature of the prolonged V_{oc} transient in the Au/TiO₂ device implies a substantially reduced tendency for recombination following the PMET process.

Previous dynamics studies on Au/TiO₂ systems have employed NP-based mesoscopic films with TiO₂ particle sizes of 10–20 nm,[6] which are too small to facilitate the formation of a depletion layer within the TiO₂ NPs.[1c, 12f] As a consequence there is no internal electric field to assist in the separation of electron-hole pairs within the semiconductor.[1c, 12f] In contrast, the dimensions of the semiconductor scaffold used in our study (0.2–2 μm) are suitable to support a depletion layer within the TiO₂ NW.[2e] Thus, the prolonged lifetimes observed for the hot electrons should result from the significant Schottky barrier ($\phi \approx 1.0$ eV) established at the Au/TiO₂ interface.[5b–f] Although this Schottky barrier tempers the transmission of hot electrons into the TiO₂ CB, once the barrier has been breached, the depletion layer within the semiconductor promotes charge separation by sweeping these hot electrons away from the Au/TiO₂ interface. Recombination is further suppressed by the absence of VB holes in TiO₂ under visible-light irradiation. Constraining the number of relaxation channels available to these transferred electrons prolongs the charge-separated state, as the only accessible recombination pathway requires traversing back through the depletion layer and across the Schottky barrier before quenching any holes trapped in the Au NPs. This rationale is supported by the direct physical contact created at the Au/TiO₂ interface via photochemical deposition (Figure 1b) and is consistent with the prolonged V_{oc} transient observed under visible-light excitation (Figure 3a). On the contrary, direct excitation of TiO₂ with UV light generates CB electrons that are not physically separate from VB holes, encouraging geminate recombination within the semiconductor. Thus, the salient feature of the PMET process involves the spatial isolation of the hot electrons in the TiO₂ CB from the holes left behind on the Au NPs (see the Supporting Information for further discussion).

Finally, since the PMET process procures a steady source of excited-state electrons exhibiting lifetimes commensurate with the timescales required for solar photochemistry,[1, 13] we evaluated the PEC activity of the Au/TiO₂ device for visible-light-driven H₂ evolution from water (see the Supporting Information). PEC experiments confirm that these hot electrons are catalytically suitable for water reduction,
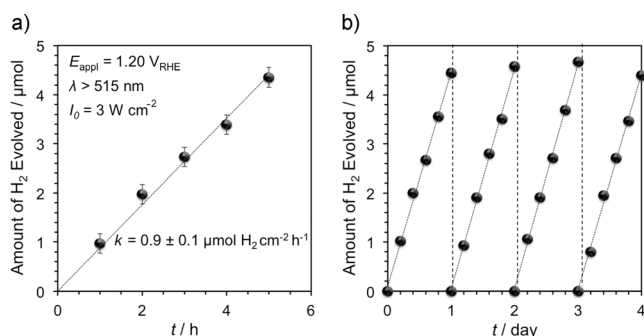
Figure 4. Visible-light-driven H_2 evolution from H_2O with a plasmonic PEC cell. a) Average H_2-production curve over time. b) PEC stability experiments performed over four consecutive days. Vertical dashed lines delineate the start/stop of each experiment.

facilitating H_2 evolution from the Pt wire cathode at a rate (k) of 0.9 ± 0.1 µmol H_2 cm^{-2} h^{-1} in the presence of methanol as a sacrificial reagent (Figure 4a). Significantly, the plasmonic photoanodes were also found to exhibit excellent PEC stability when subjected to repeated 5 h photocatalytic cycling experiments, as shown in Figure 4b. We note that the TiO_2-only device does not produce H_2 when subjected to identical experimental conditions (Figure S6), further demonstrating the unique characteristics of hot electrons for solar photochemistry.[14]

In summary, we used PEC techniques to probe hot electron dynamics within Au/TiO_2 heterojunctions in situ and confirm the existence of PMET in these plasmonic photoanodes. We discovered that the lifetimes of hot electrons transferred to the TiO_2 CB are 1–2 orders of magnitude longer than those of CB electrons generated directly within the TiO_2 support via UV excitation. Such marked differences in lifetime are attributed to the Schottky barrier at the Au/TiO_2 interface, which impedes recombination following PMET to the TiO_2 CB. We further harnessed these long-lived electrons for visible-light-driven H_2 evolution from water, demonstrating their potential for solar photocatalysis. These results highlight the merits of the PMET strategy for extending the excited-state lifetimes of charge carriers within PEC devices, while simultaneously sensitizing the semiconductor scaffold to sub-band gap light. We anticipate improved photocatalytic efficiencies for a variety of kinetically hindered chemical reactions if plasmonic-metal/semiconductor heterostructures can be appropriately engineered to exploit the PMET process.

[1] a) N. S. Lewis, D. G. Nocera, *Proc. Natl. Acad. Sci. USA* **2006**, *103*, 15729–15735; b) A. J. Cowan, J. R. Durrant, *Chem. Soc. Rev.* **2013**, *42*, 2281–2293; c) M. Grätzel, *Nature* **2001**, *414*, 338–344.

[2] a) S. Linic, P. Christopher, D. B. Ingram, *Nat. Mater.* **2011**, *10*, 911–921; b) S. C. Warren, E. Thimsen, *Energy Environ. Sci.* **2012**, *5*, 5133–5146; c) X. Lang, X. Chen, J. Zhao, *Chem. Soc. Rev.* **2014**, *43*, 473–486; d) A. Primo, A. Corma, H. García, *Phys. Chem. Chem. Phys.* **2011**, *13*, 886–910; e) Z. Zhang, J. T. Yates, Jr., *Chem. Rev.* **2012**, *112*, 5520–5551.

[3] a) Y. Tian, T. Tatsuma, *J. Am. Chem. Soc.* **2005**, *127*, 7632–7637; b) Y. Nishijima, K. Ueno, Y. Kotake, K. Murakoshi, H. Inoue, H. Misawa, *J. Phys. Chem. Lett.* **2012**, *3*, 1248–1252; c) C. Gomes Silva, R. Juárez, T. Marino, R. Molinari, H. García, *J. Am. Chem. Soc.* **2011**, *133*, 595–602; d) S. Mubeen, J. Lee, N. Singh, S. Kramer, G. D. Stucky, M. Moskovits, *Nat. Nanotechnol.* **2013**, *8*, 247–251; e) Y. Pu, G. Wang, K. Chang, Y. Ling, Y. Lin, B. C. Fitzmorris, C. Liu, X. Lu, Y. Tong, J. Z. Zhang, Y. Hsu, Y. Li, *Nano Lett.* **2013**, *13*, 3817–3823; f) Z. Bian, T. Tachikawa, P. Zhang, M. Fujitsuka, T. Majima, *J. Am. Chem. Soc.* **2014**, *136*, 458–465; g) A. Primo, T. Marino, A. Corma, R. Molinari, H. García, *J. Am. Chem. Soc.* **2011**, *133*, 6930–6933.

[4] a) E. Thimsen, F. Le Formal, M. Grätzel, S. C. Warren, *Nano Lett.* **2011**, *11*, 35–43; b) I. Thomann, B. A. Pinaud, Z. Chen, B. M. Clemens, T. F. Jaramillo, M. L. Brongersma, *Nano Lett.* **2011**, *11*, 3440–3446; c) H. Gao, C. Liu, H. E. Jeong, P. Yang, *ACS Nano* **2012**, *6*, 234–240; d) D. B. Ingram, S. Linic, *J. Am. Chem. Soc.* **2011**, *133*, 5202–5205; e) J. Li, S. K. Cushing, P. Zheng, F. Meng, D. Chu, N. Wu, *Nat. Commun.* **2013**, *4*, 2651–2658; f) Q. Zhang, D. Q. Lima, I. Lee, F. Zaera, M. Chi, Y. Yin, *Angew. Chem. Int. Ed.* **2011**, *50*, 7088–7092; *Angew. Chem.* **2011**, *123*, 7226–7230; g) R. Long, K. Mao, M. Gong, S. Zhou, J. Hu, M. Zhi, Y. You, S. Bai, J. Jiang, Q. Zhang, X. Wu, Y. Xiong, *Angew. Chem. Int. Ed.* **2014**, *53*, 3205–3209; *Angew. Chem.* **2014**, *126*, 3269–3273.

[5] a) M. W. Knight, H. Sobhani, P. Nordlander, N. J. Halas, *Science* **2011**, *332*, 702–704; b) Y. K. Lee, C. H. Jung, J. Park, H. Seo, G. A. Somorjai, J. Y. Park, *Nano Lett.* **2011**, *11*, 4251–4255; c) A. O. Govorov, H. Zhang, Y. K. Gun'ko, *J. Phys. Chem. C* **2013**, *117*, 5548–5552; d) S. Mubeen, G. Hernandez-Sosa, D. Moses, J. Lee, M. Moskovits, *Nano Lett.* **2011**, *11*, 5548–5552; e) R. Long, O. V. Prezhdo, *J. Am. Chem. Soc.* **2014**, *136*, 4343–4354; f) E. W. McFarland, J. Tang, *Nature* **2003**, *421*, 616–618.

[6] a) A. Furube, L. Du, K. Hara, R. Katoh, M. Tachiya, *J. Am. Chem. Soc.* **2007**, *129*, 14852–14853; b) J. Sá, G. Tagliabue, P. Friedli, J. Szlachetko, M. H. Rittman-Frank, F. G. Santomauro, C. J. Milne, H. Sigg, *Energy Environ. Sci.* **2013**, *6*, 3584–3588; c) K. Wu, W. E. Rodríguez-Córdoba, Y. Yang, T. Lian, *Nano Lett.* **2013**, *13*, 5255–5263; d) J. B. Priebe, M. Karnahl, H. Junge, M. Beller, D. Hollmann, A. Brückner, *Angew. Chem. Int. Ed.* **2013**, *52*, 11420–11424; *Angew. Chem.* **2013**, *125*, 11631–11635.

[7] A. Linsebigler, G. Lu, J. T. Yates, Jr., *Chem. Rev.* **1995**, *95*, 735–758.

[8] W. Hou, S. B. Cronin, *Adv. Funct. Mater.* **2013**, *23*, 1612–1619.

[9] a) M. G. Walter, E. L. Warren, J. R. McKone, S. W. Boettcher, Q. Mi, E. M. Santori, N. S. Lewis, *Chem. Rev.* **2010**, *110*, 6446–6473; b) B. Liu, E. S. Aydil, *J. Am. Chem. Soc.* **2009**, *131*, 3985–3990; c) J. M. Foley, M. L. Price, J. I. Feldblyum, S. Maldonado, *Energy Environ. Sci.* **2012**, *5*, 5203–5220; d) M. Law, L. E. Greene, J. C. Johnson, R. Saykally, P. Yang, *Nat. Mater.* **2005**, *4*, 455–459.

[10] a) S. C. Chan, M. A. Barteau, *Langmuir* **2005**, *21*, 5588–5595; b) Y. Matsumoto, S. Ida, T. Inoue, *J. Phys. Chem. C* **2008**, *112*, 11614–11616; c) X. Huang, X. Qi, Y. Huang, S. Li, C. Xue, C. Gan, F. Boey, H. Zhang, *ACS Nano* **2012**, *4*, 6196–6202.

[11] a) J. Bisquert, A. Zaban, M. Greenshtein, I. Mora-Seró, *J. Am. Chem. Soc.* **2004**, *126*, 13550–13559; b) A. Zaban, M. Greenshtein, J. Bisquert, *ChemPhysChem* **2003**, *4*, 859–864; c) B. H. Meekins, P. V. Kamat, *ACS Nano* **2009**, *3*, 3437–3446.

[12] a) J. R. Swierk, T. E. Mallouk, *Chem. Soc. Rev.* **2013**, *42*, 2357–2387; b) X. Feng, K. Zhu, A. J. Frank, C. A. Grimes, T. E. Mallouk, *Angew. Chem. Int. Ed.* **2012**, *51*, 2727–2730; *Angew.*

Chem. **2012**, *124*, 2781–2784; c) L. Bertoluzzi, I. Herraiz-Cardona, R. Gottesman, A. Zaban, J. Bisquert, *J. Phys. Chem. Lett.* **2014**, *5*, 689–694; d) M. Yang, B. Ding, S. Lee, J. Lee, *J. Phys. Chem. C* **2011**, *115*, 14534–14541; e) Y. J. Hwang, C. Han, B. Liu, P. Yang, *ACS Nano* **2012**, *6*, 5060–5069; f) A. Hagfeldt, M. Grätzel, *Chem. Rev.* **1995**, *95*, 49–68.

[13] a) Z. Huang, Y. Lin, W. Rodríguez-Córdoba, K. J. McDonald, K. S. Hagen, K. S. Choi, B. S. Brunschwig, D. G. Musaev, C. L. Hill, D. Wang, T. Lian, *Energy Environ. Sci.* **2012**, *5*, 8923–8926; b) R. Liu, G. Yuan, C. L. Joe, T. E. Lightburn, K. L. Tan, D.

Wang, *Angew. Chem. Int. Ed.* **2012**, *51*, 6709–6712; *Angew. Chem.* **2012**, *124*, 6813–6816; c) R. J. Dillon, J. Joo, F. Zaera, Y. Yin, C. J. Bardeen, *Phys. Chem. Chem. Phys.* **2013**, *15*, 1488–1496; d) F. Le Formal, S. R. Pendlebury, M. Cornuz, S. D. Tilley, M. Gratzel, J. R. Durrant, *J. Am. Chem. Soc.* **2014**, *136*, 2564–2574.

[14] a) S. Linic, P. Christopher, H. Xin, A. Marimuthu, *Acc. Chem. Res.* **2013**, *46*, 1890–1899; b) S. Mukherjee, L. Zhou, A. M. Goodman, N. Large, C. Ayala-Orozco, Y. Zhang, P. Nordlander, N. J. Halas, *J. Am. Chem. Soc.* **2014**, *136*, 64–67.